Ultraviolet Light-Induced Hydrophilicity Effect on $TiO_2(110)(1\times1)$. Dominant Role of the Photooxidation of Adsorbed Hydrocarbons Causing Wetting by Water Droplets

Tykhon Zubkov,[†] Dirk Stahl,[‡] Tracy L. Thompson, Dimitar Panayotov, Oliver Diwald,[§] and John T. Yates, Jr.*

Surface Science Center, Department of Chemistry, University of Pittsburgh, Pittsburgh, Pennsylvania 15260

Received: March 23, 2005; In Final Form: May 31, 2005

The UV photoproduction of a hydrophilic $TiO_2(110)(1\times1)$ surface has been investigated in a pressurized ultrahigh vacuum apparatus under controlled conditions of hydrocarbon concentration in oxygen gas at 1 atm pressure. Water droplet contact angles have been measured continuously as the droplet is exposed to UV irradiation, yielding the first observations of a sudden wetting process during irradiation. Using hexane as a model hydrocarbon, it is found that when low partial pressures of hexane are present, the sudden onset of surface wetting occurs during UV irradiation after an induction period under photooxidation conditions. The induction period to reach the critical condition for sudden wetting increases when the partial pressure (and equilibrium surface coverage) of hexane is increased. These results indicate that the removal of adsorbed hydrocarbons by photooxidation is the critical factor leading to the UV-induced hydrophilicity phenomenon on TiO_2. The phenomenon does not occur in the absence of O_2 gas. A concept concerned with kinetic screening of the TiO_2-H_2O interface from O_2 by water droplets is presented to explain the observation of sudden wetting in our experiments, compared to gradual wetting which is observed following UV irradiation in all other experiments reported in the literature. Complementary infrared spectroscopy measurements of the effect of UV irradiation in an O_2 atmosphere on adsorbed Ti−OH groups and on adsorbed H_2O on the surface of a high-area TiO_2 powder show that no spectroscopic changes occur. This indicates that UV-induced changes in the −OH coverage or the nature of −OH bonding to TiO_2, as suggested by others, cannot be used to explain the photoinduced hydrophilicity effect.

I. Introduction

The observation of the UV-induced hydrophilicity phenomenon on TiO_2 surfaces in air has attracted widespread scientific and technological interest, and many publications have focused on this effect.[1−17] Summarizing the massive amount of literature available on this topic, three hypotheses to explain this effect have been offered: (1) wetting is caused by the removal of hydrophobic layers of hydrocarbons or other carbonaceous species by TiO_2-mediated photooxidation, leading to the attractive interaction of water with clean TiO_2;[1−7,17] (2) wetting is caused by the photoproduction of surface defects which then become hydroxylated by water dissociation, making hydrophilic surface sites;[8−12,15,16] (3) wetting is caused by the photoinduced rupturing of Ti−O bonds in bridged >OH groups on TiO_2.[4,13]

All of the water contact angle experiments leading to the postulates for the origin of the UV-induced hydrophilic effect listed above have been carried out in air or other atmospheres where control of hydrocarbon surface impurities has not been achieved. All of these experiments have reported a *gradual* decrease in water contact angle as UV irradiation takes place, and many studies report a gradual increase in contact angle after illumination is interrupted and exposure to the ambient atmosphere continues. In this paper, we show, for the first time, that under highly controlled atmospheric conditions the UV-induced hydrophilicity effect is a *sudden* effect which takes place during irradiation after an induction period required to remove adsorbed hydrocarbons by photooxidation. We also show that preferential photooxidation occurs beyond the water droplet perimeter, leading to a critical condition at the droplet perimeter which causes very rapid droplet spreading. This indicates that partial screening from O_2 of the water−TiO_2 interface under the droplet decreases the rate of hydrocarbon photooxidation under the droplet.

II. Experimental Methods

A. UV-Induced Hydrophilicity on Rutile Single-Crystal $TiO_2(110)$. To control the surface cleanliness of the $TiO_2(110)$-(1×1) single crystal surface, a special bakeable ultrahigh vacuum (UHV) apparatus has been constructed, as shown in Figure 1. This apparatus provides a novel method for contact angle measurements under highly controlled surface and atmospheric conditions, extending the large number of earlier studies made in air under relatively uncontrolled conditions. The vacuum system is rapidly pumped by ion pumps, turbo pumps, a cryopump, and a titanium sublimation pump. It consists of two interconnected chambers operating at a base pressure of $(2-5)\times10^{-10}$ mbar. Care was taken to exclude room light from the TiO_2 surface during the experiments. An atomically clean single crystal of TiO_2, mounted on a translating manipulator (Figure 1b), is prepared by Ar^+ sputtering (1.5 keV). The crystal is then

* Corresponding author. E-mail: jyates@pitt.edu.
[†] Present address: Environmental Molecular Sciences Laboratory, Pacific Northwest National Laboratory, P.O. Box 999/K8-88, Richland, Washington 99352.
[‡] Present address: Leica Microsystems Lithography GMbH, Goeschwitzer Strasse 25, 07745 Jena, Germany.
[§] Present address: Institut für Materialchemie der TU-Wien, Bereich Physikalische Chemie, Veterinärplatz 1/GA, A-1210 Wien, Austria.

10.1021/jp058101c CCC: $30.25
Published on Web 07/27/2005

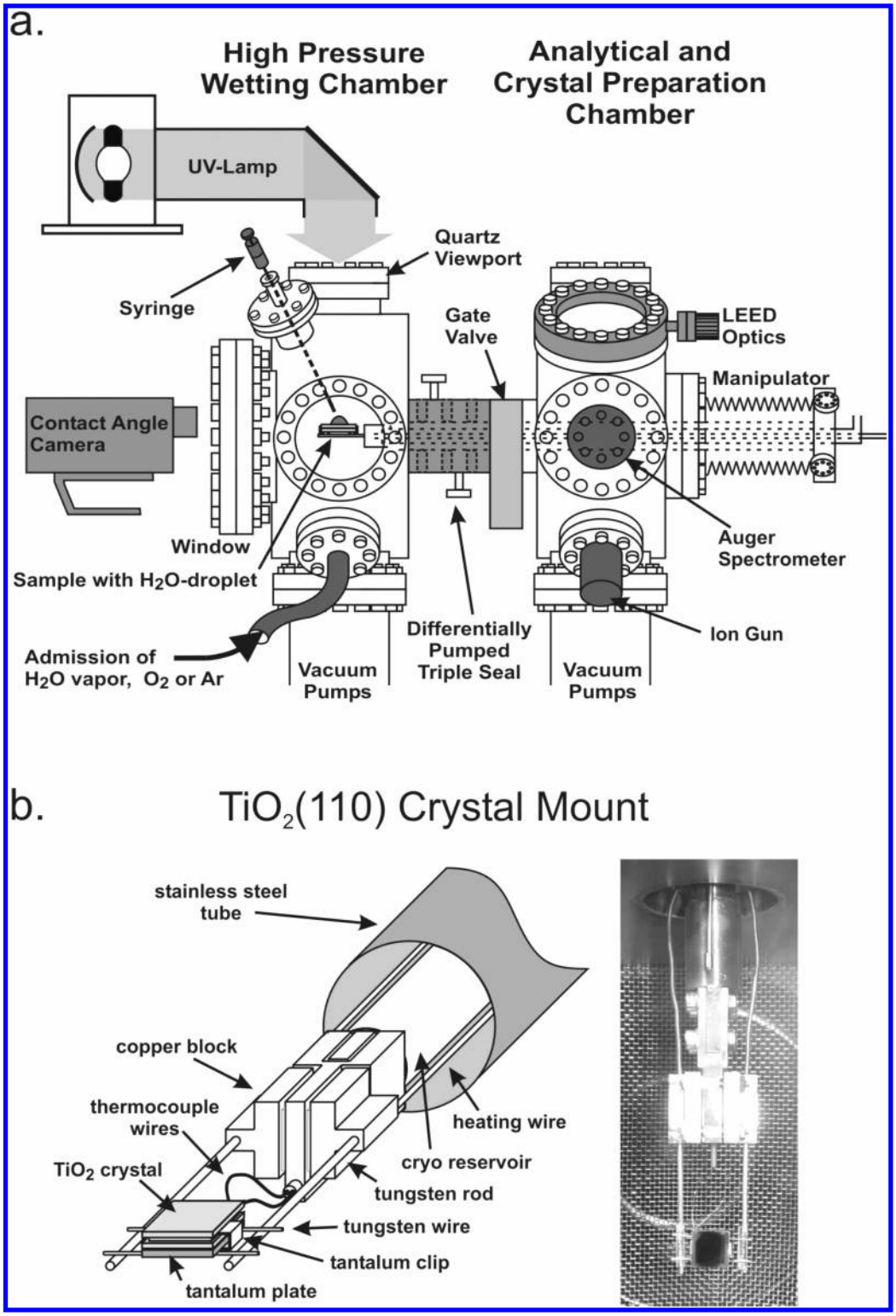

Figure 1. (a) Apparatus for wetting studies of ultrahigh-vacuum-prepared TiO_2 surfaces under controlled atmospheres. To place water droplets onto the sample with a syringe and to measure water contact angles, the wetting chamber is pressurized to 1 atm while the analytical and crystal-preparation chamber remains at ultrahigh vacuum. (b) Schematic drawing and photographic image of the sample mount specifically designed to work with the triple seal mechanism separating the two chambers. It allows for electrical heating in the analytical and crystal-preparation chamber to above 900 K with attached W heating leads and cooling with a cryoreservoir through the same W leads and insulating sapphire wafers.

oxidized at 900 K and cooled to room temperature under O_2 flux to produce the (1×1) defect-free surface in the analytical and crystal-preparation chamber.[18] The analytical and crystal-preparation chamber is equipped with a PHI 10-155 CMA Auger spectrometer, a Specs reverse view low-energy electron diffraction (LEED) diffractometer, a SRS RGA 200 quadrupole mass spectrometer, and a capillary array gas doser.[19] The crystal $(10 \times 10 \times 1\ mm^3)$ is mounted on a Ta plate that may be heated electrically above 900 K by attached W heating leads or cooled by a cryoreservoir through the same leads. The crystal temperature is accurately measured by an embedded type K thermocouple,[20] and its temperature may be controlled electronically. The atomically clean and ordered crystal is then transferred into the high-pressure chamber through a gate valve and a differ-

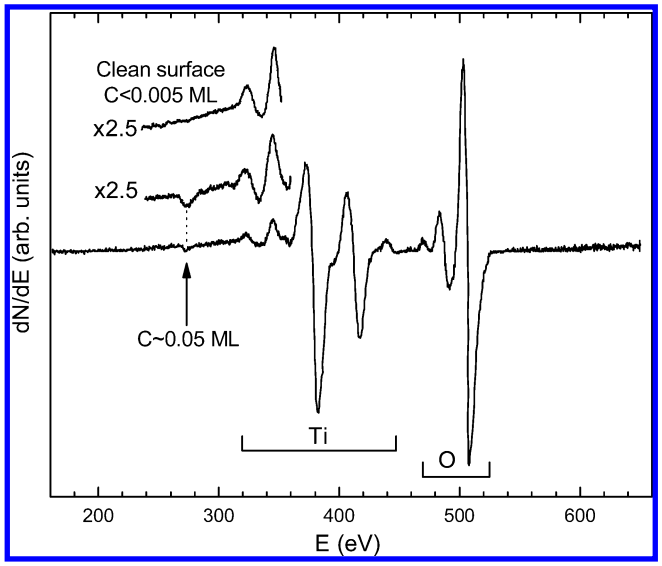

Figure 2. Typical Auger spectrum of a TiO_2(110) sample after wetting measurements. The residual carbon signal can be seen in a magnified spectral region. For comparison, a similar magnified spectral region for the clean TiO_2(110) sample shows no detectable carbon.

entially pumped Teflon sliding seal,[19] which isolates the two chambers. To minimize droplet evaporation and to ensure 100% relative humidity during the wetting experiments, the chamber was pressurized, first, with pure H_2O vapor and, then, with water-saturated O_2. The resulting excess moisture precipitated as fog droplets on the inside of the chamber viewports. Highly pure O_2 (Penn Oxygen, 99.9999% pure; hydrocarbons < 0.05 ppm) is saturated with H_2O vapor above the water surface in a glass bulb and slowly admitted to the high-pressure chamber through the bakeable stainless steel gas handling line; it will be demonstrated later that O_2 is needed to produce the hydrophilic effect. Pressure is measured with MKS Baratrons (0−1000 and 0−10 Torr). The combination of these two chambers allows for preparation and characterization of the atomically clean surface and subsequent transfer under UHV into a chamber that can be filled to atmospheric pressures (with a controlled atmosphere of O_2, water vapor, and hydrocarbons). Furthermore, crystal transfer back into the surface analysis chamber is easily achieved after it has been used for contact angle measurements.

Contact angle measurements were made by the sessile drop method. The type I Reagent Grade water used in these experiments was prepared by distillation and deionization in a commercial purifier (Barnstead NANOpure Infinity) and exhibited a specific resistivity of 18.2 MΩ cm. Water droplets were introduced to the TiO_2 crystal using a stainless steel syringe needle that passes through a flange-mounted stainless steel entry tube which can be sealed off when necessary. To ensure cleanliness, the syringe and needle were passivated and cleaned by boiling in H_2O_2(aq) and ultrapure water for hours. Because of a slight excess of pressure maintained inside the wetting chamber, flowing gas escapes continuously through the entry tube during the measurements of contact angle. As shown in Figure 2, little contamination was detected (using Auger spectroscopy) on the TiO_2 surface after the water droplet had evaporated. Experiments comparing the clean crystal and the water-treated crystal showed that the residual nonvolatile C coverage was near 0.05 monolayers (1 ML = 2.08×10^{15} C atoms cm^{-2})[21] following H_2O droplet deposition at 1 atm, evacuation, and crystal translation back into the analytical chamber for Auger spectroscopy. The calculation uses the ratio I_C/I_O of the C (271 eV) transition intensity to the O (510 eV) transition intensity and the appropriate electron mean free path in TiO_2[22] and elemental sensitivity factors at the 42° takeoff angle[23] present in our Auger electron optics. Assuming that carbon is deposited exclusively on the outermost TiO_2(110) surface layer, all the factors taken into account yield the following expression for carbon concentration: $\theta_C(\mathrm{ML}) = 4.92 I_C/I_O$. These measurements indicate that the *nonvolatile* carbon contamination is negligible following TiO_2 crystal exposure to liquid H_2O droplets at 1 atm. Studies of other regions of the Auger spectrum after contact with H_2O(l) indicated the absence of any other elements on the surface within 0.01 ML.

In experiments designed to measure the effect of added hexane on the hydrophilicity phenomenon, small measured quantities of hexane vapor (98% purity) were introduced into the chamber containing the cleaned TiO_2(110) crystal, followed by admission of H_2O-saturated O_2(g) to 1 atm of pressure. The mass spectrometer was employed to sample the hexane/O_2 gas mixture by leaking a small sample of the gas mixture into the analytical chamber.

Images of the H_2O droplets (~2 mm diameter) during UV irradiation were recorded at 0.5−1 s intervals with a VCA Optima CCD camera, and the contact angle was mathematically fitted to the meniscus shape with dedicated software (VCA version 1.75, AST Products, Inc.). Because of the nature of the operator input of the meniscus coordinates, there is an inherent uncertainty of the contact angles (standard deviation of ±1°). This uncertainty rapidly increases for small angles (<7−9°) where it is difficult to determine the droplet boundaries.

LEED measurements (electron beam energy = 150 eV) were made and recorded with a CCD camera both before and after wetting the surface with the water droplet. The image capturing and quantitative processing were done using astronomical software (CCDOPS version 4.12-NT, Santa Barbara Instruments Group, and AlP4WIN version 1.1.4, Willman-Bell, Inc.). The coherence length of the electrons was 50−100 Å, meaning that the LEED intensity may be interpreted for regions of this size or for smaller sizes. We observed a reduction of LEED beam intensity following wetting and H_2O evaporation, as shown in Figure 3a and b. The average intensity reduction in the five representative beams labeled in Figure 3a after wetting and evaporation is 2.2 ± 0.3, which indicates an overall increase in the surface disorder or possibly the presence of small coverages of carbon as measured by Auger spectroscopy. This is consistent with recent observations with scanning tunneling microscopy (STM) of limited erosion (nanometer pits) of the TiO_2(110) surface with exposure to liquid H_2O.[24] However, we observed no change in the half-width of the LEED beams following contact with H_2O droplets and H_2O evaporation, as shown in Figure 3c and d, indicating that the surface retains ordered regions that are larger in size than the coherence length of the electrons (50−100 Å). The continued existence of the ordered surface after exposure to H_2O(l) suggests that massive reconstruction of the surface does not occur upon exposure to H_2O(l) over TiO_2 surface regions of sizes below 50−100 Å. Effects such as solubilization of TiO_2, followed by TiO_2 redeposition upon water vaporization, are therefore insignificant as the water droplet contacts the crystal surface.

The UV source employed for these measurements is a Hg arc lamp (Oriel, 500 W) that is filtered with a 10 cm path length water filter to remove IR radiation. Ultraviolet−visible radiation in the 280−600 nm range (photon energy = 2.1−4.4 eV) is directed through a sapphire window to the sample. The wattage received by the crystal (0.049 W cm^{-2}) was measured with a

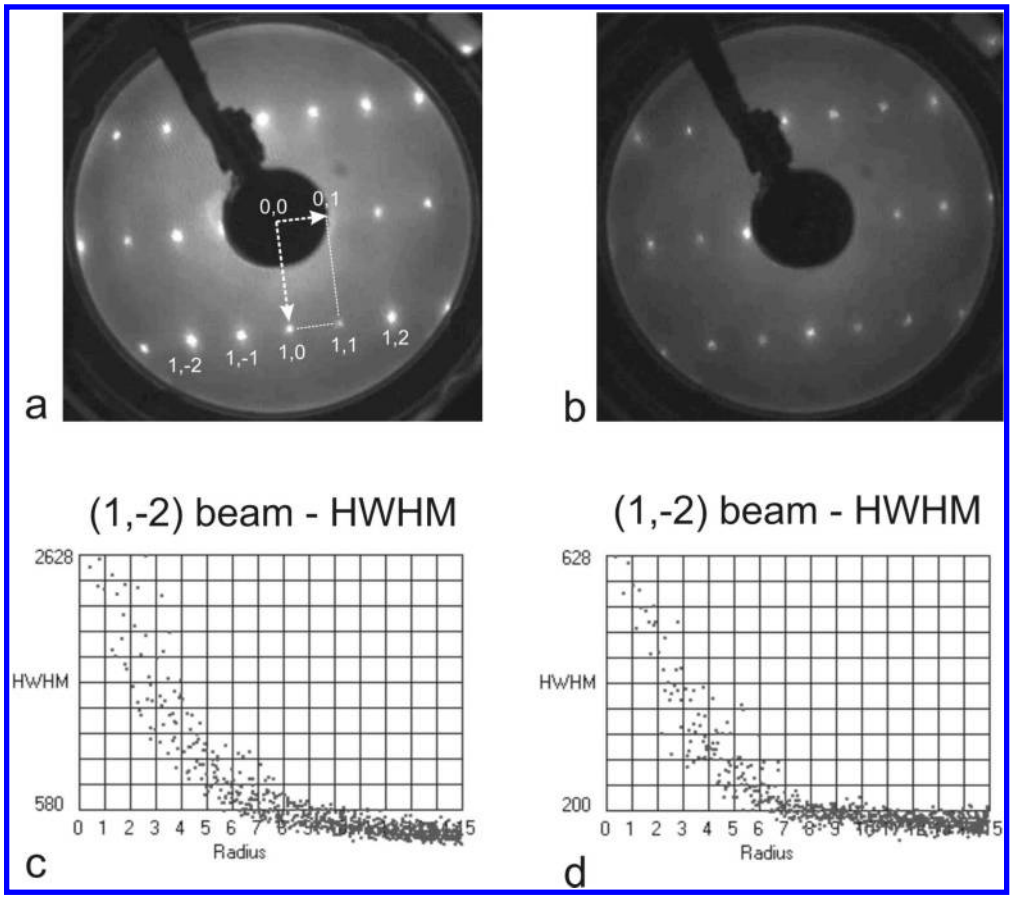

Figure 3. (a and b) LEED patterns recorded at 115 V (a) from a clean $TiO_2(110)(1\times1)$ surface and (b) from a TiO_2 surface after wetting experiments. Reciprocal lattice vectors and reflexes are indicated. (c) Profile of the (1,−2) LEED reflex for the clean surface. (d) LEED reflex profile after wetting experiments. The reflex radius is in arbitrary units.

ThorLabs power meter (model D3MM) and corresponds to a light flux of 1.1×10^{17} photons cm^{-2} s^{-1}, weighted for the spectral irradiance of the UV lamp. A low-pass filter was used to cut off radiation above 4.4 eV ($\lambda < 280$ nm) to eliminate the possibility of ozone production in the chamber.[25] The crystal is observed to warm by 1−5 K during UV irradiation.

B. Transmission IR Spectroscopy Studies. Experiments on TiO_2 in the presence of O_2(g) and in a vacuum were performed with UV−visible irradiation in the range 2.1−6.2 eV, using an identical light source to that used in the contact angle experiments. Degussa P-25 TiO_2 (70% anatase; 30% rutile; 50 ± 15 m^2 g^{-1}) was employed, and the powdered sample was hydrostatically pressed into a transparent tungsten mesh grid which was inserted into a stainless steel ultrahigh vacuum IR cell (base pressure $= 10^{-8}$ mbar).[20,26] Oxidation at 958 K, followed by cooling in O_2, was carried out to prepare the sample in a manner almost identical to that used for the $TiO_2(110)$ surface. Transmission IR spectra were acquired at 4 cm^{-1} resolution using 200 scans.

III. Experimental Results

A. Contact Angle Measurements in O_2 at 1 atm for Different Gas-Phase Hexane Concentrations. Figure 4 shows representative water contact angle measurements made at a hexane gas concentration of 120 ppm as UV irradiation occurs. A slow, small decrease in contact angle occurs initially as a result of slow evaporation of the water droplet during the measurement, but after an induction period of 154 s, the water droplet is observed to completely wet the surface within one image sampling period (1 s). The droplet contact angle decreases abruptly to below the measurement limit of about 7−9°. This sudden wetting phenomenon is characteristic of all measurements made with hexane vapor in the 30−360 ppm range in the O_2 atmosphere. Figure 5 shows the observed water contact angle as a function of irradiation time for three representative experiments at different added hexane gas concentrations.

Figure 6 shows a plot of the observed wetting delay as a function of the added hexane gas concentration. At zero hexane concentration, five measurements are shown in which the average induction period is 3 s. Three of these measurements yielded 0 s induction periods. The measurements in Figure 6 show a definite correlation of the wetting delay with the hexane concentration, although the scatter in the data is fairly high. We believe that experimental factors which determine the wetting delay (such as exact crystal temperature, exact hexane concentration, and exact droplet size) may contribute to rather large uncertainties in the measurement of the wetting delay. It is noted that the initial contact angle is relatively insensitive to the hexane gas concentration. Probably at low hexane gas concentrations, present as a trace gas contaminant even when no hexane has been added to the pure O_2, a fraction of a monolayer of hexane will be adsorbed prior to irradiation and, thus, will determine the contact angle. At low hexane gas concentration, the adsorbed hexane layer will be more rapidly depleted by photooxidation due to the lower arrival flux of hexane from the gas.

B. Droplet Screening Effect. An experiment was carried out in a water vapor-saturated [O_2 (10%) + Ar (90%)] atmosphere to determine whether photooxidation effects under the water

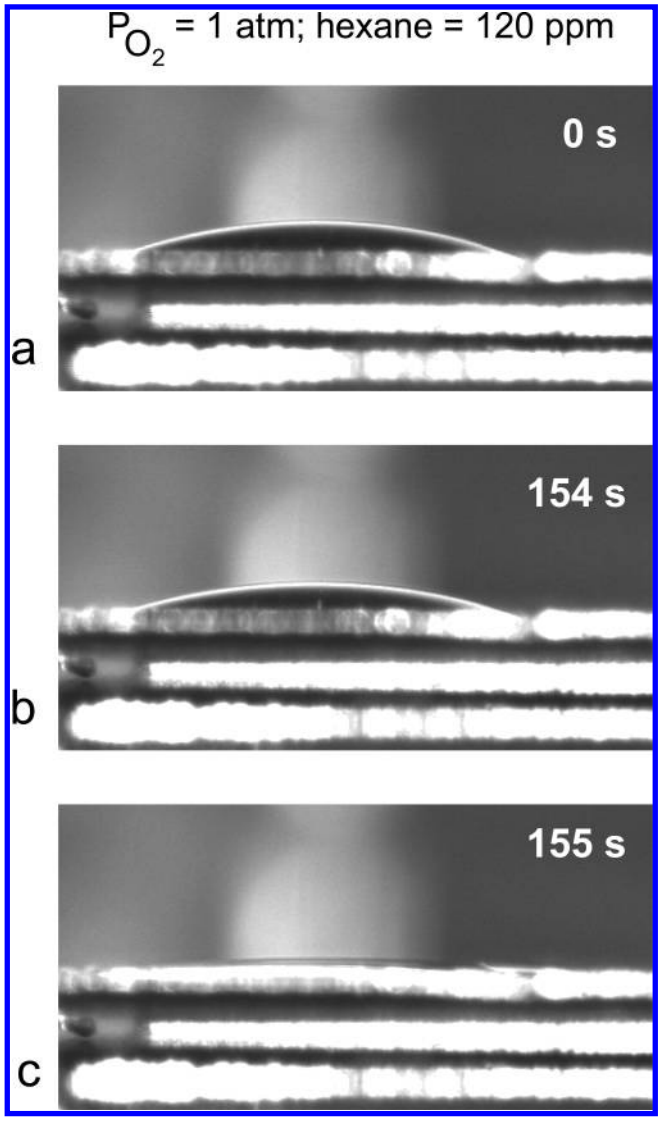

Figure 4. Video capture frames showing a water droplet in an O_2−hexane (120 ppm) atmosphere under UV light for different irradiation times: (a) 0 s; (b) 154 s; (c) 155 s.

droplet differ from those on exterior TiO_2 surface regions beyond the droplet perimeter. In this experiment, O_2 gas (99.98% pure, containing hundreds of ppm of impurity hydrocarbon) was employed. Figure 7 shows a droplet which has been irradiated for 10 s (in the wetting delay period) where little contact angle change has occurred. Following irradiation, the droplet size was increased by adding a second droplet. Immediate spreading of the enlarged droplet occurs. This indicates that photooxidation of adsorbed hydrocarbons takes place preferentially in TiO_2 surface regions beyond the droplet perimeter which are unscreened by bulk water. When the droplet is advanced into these unscreened regions, wetting occurs immediately.

C. Role of Oxygen. To check that the photoinduced hydrophilicity effect requires O_2, a series of experiments were performed under conditions where background hydrocarbons, introduced from lower purity O_2, were present. Using 99.98% pure O_2, an experiment was performed in which irradiation was carried out in a water vapor-saturated [O_2 (10%) + Ar (90%)] atmosphere. Following various times of irradiation, water droplets were added onto the dry surface of the crystal and the contact angle was measured, as shown in Figure 8. The contact angle during the initial 50 s of irradiation time gradually drops to near the measurement limit. The experiment was repeated in pure Ar (BOC Edwards, 99.9999% pure), and the contact angle was observed to be invariant as the UV irradiation time was increased. These measurements demonstrate that the TiO_2 UV-induced hydrophilicity phenomenon requires O_2.

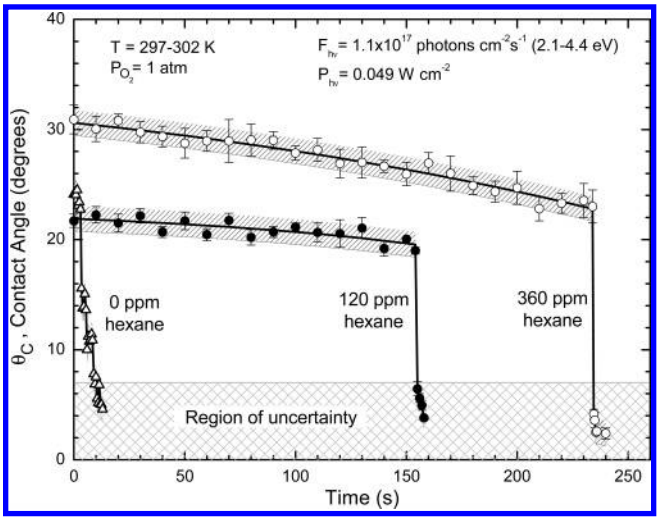

Figure 5. Water contact angle evolution during UV irradiation in an oxygen atmosphere with different hexane concentrations. During the wetting delay, the contact angle slowly decreases due to slight droplet evaporation. Error bars correspond to the average deviation of the contact angles measured on the two sides of the droplet from the average value. Shaded regions around the curves represent the ±1° error of the angle measurement processing.

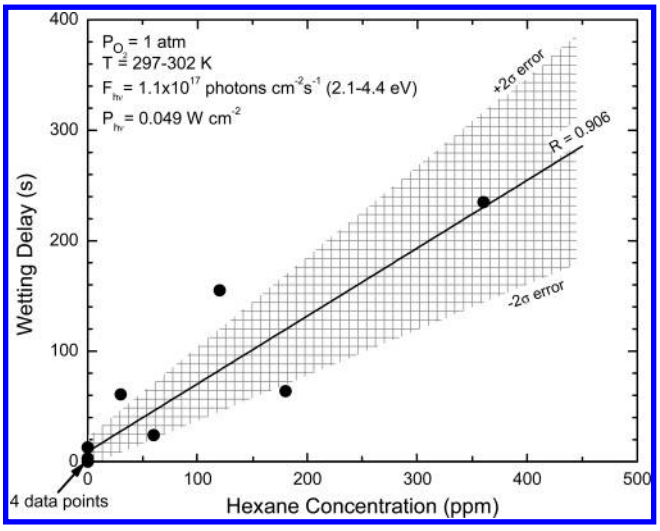

Figure 6. Correlation of the wetting delay with hexane vapor concentration in O_2(g) at 1 atm. The line corresponds to the linear fit with a correlation coefficient $R = 0.906$ and with $\pm 2\sigma$ deviation in slope depicted as the shaded region.

D. Transmission Infrared Spectroscopy Studies of the UV Effect on H_2O and Ti−OH on TiO_2. Using methods developed in this laboratory for the study by IR spectroscopy of UV-induced photochemical phenomena on high-area oxides, including TiO_2 powders,[20] an exploratory experiment was performed to determine whether chemisorbed H_2O or Ti−OH surface groups are affected by UV irradiation.

Figure 9a shows the transmission IR spectrum obtained in the −OH stretching region after H_2O adsorption at 300 K and cooling to 153 K. Working at this low-temperature prevents H_2O evaporation and dehydroxylation effects which would occur at 300 K under vacuum. Above ~3600 cm^{-1}, Ti−OH modes due to isolated groups are seen.[27−31] Below 3600 cm^{-1}, the

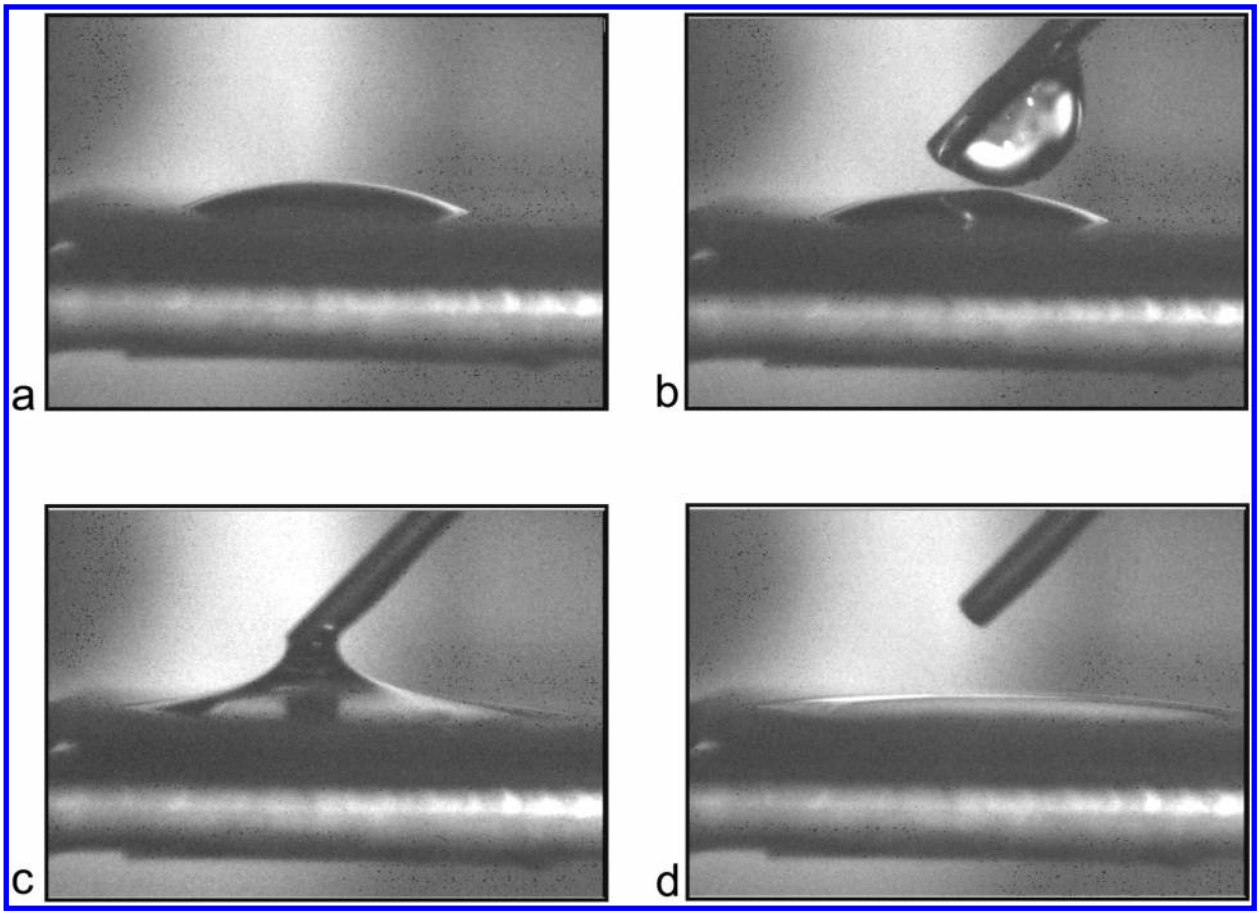

Figure 7. Video capture frames showing a water droplet in an Ar + 10% O_2 atmosphere: (a) before UV irradiation; (b−d) after adding more water to the same droplet after 10 s of UV irradiation.

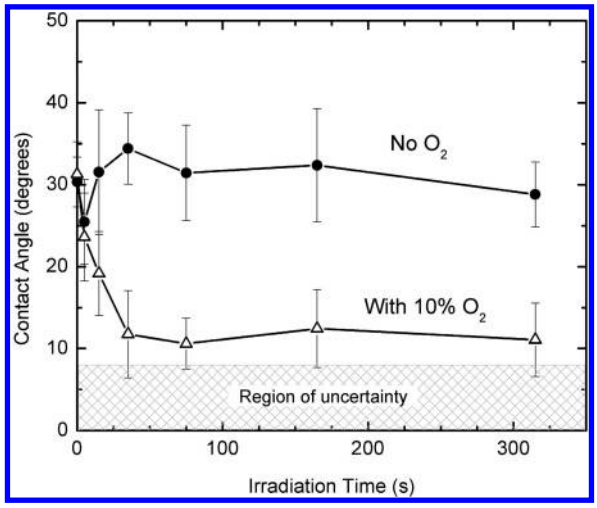

Figure 8. Effect of UV irradiation on a $TiO_2(110)$ surface in a water-saturated Ar atmosphere compared to a water-saturated Ar + 10% O_2 atmosphere. Error bars correspond to the standard deviation of 12 contact angle measurements for each data point.

broad band contains contributions from hydrogen-bonded (associated) Ti−OH groups and from hydrogen-bonded water molecules.[27−31] The sample was exposed for 200 min to 16 Torr of O_2(g) and to UV irradiation, and the IR spectrum was again recorded. No significant changes were observed in the 3800−3000 cm^{-1} region, as may be seen by the inset to Figure 9a, which amplifies the difference in the absorbance between the spectra. A similar experiment was done in the absence of O_2(g), as shown in Figure 9b. Again, no observable spectral effects are seen. These results indicate that the surface coverage and the surface bonding of Ti−OH groups and of adsorbed H_2O molecules are not influenced by UV irradiation.

IV. Discussion

A. Rationale for Experiments. These experiments provide a quantitative probe of the phenomenon of the UV-induced hydrophilicity of TiO_2 surfaces where the following parameters have been controlled to the limit of experimental capability: (1) a $TiO_2(110)$ single crystal which is atomically clean and ordered is the substrate investigated, and the substrate surface character has been confirmed by physical measurements; (2) a known, low natural level of surface oxygen vacancy defects is present following high-temperature oxidation;[32] (3) a highly controlled oxygen atmosphere is employed containing small added concentrations of hexane gas, a representative hydrocarbon; (4) highly purified water, which is shown to introduce little carbon or other surface contamination, is employed; and (5) a known fluence of UV irradiation with a known spectral distribution of wavelengths is employed.

In addition to the rigid control of the parameters listed above, measurements of the water contact angle have been continuously made by CCD imaging *during* UV exposure. This procedure mimics the actual conditions *which occur in the field* where hydrophilicity effects take place on TiO_2 surfaces containing water droplets during continuous exposure to light. Other contact angle measurements (including some of our own as in Figure 8) have been made by the addition of water droplets to surfaces which have received various UV exposures *prior* to droplet addition. Such wetting experiments invariably do not exhibit the induction period observed prior to wetting, in contrast to the experiments presented here.

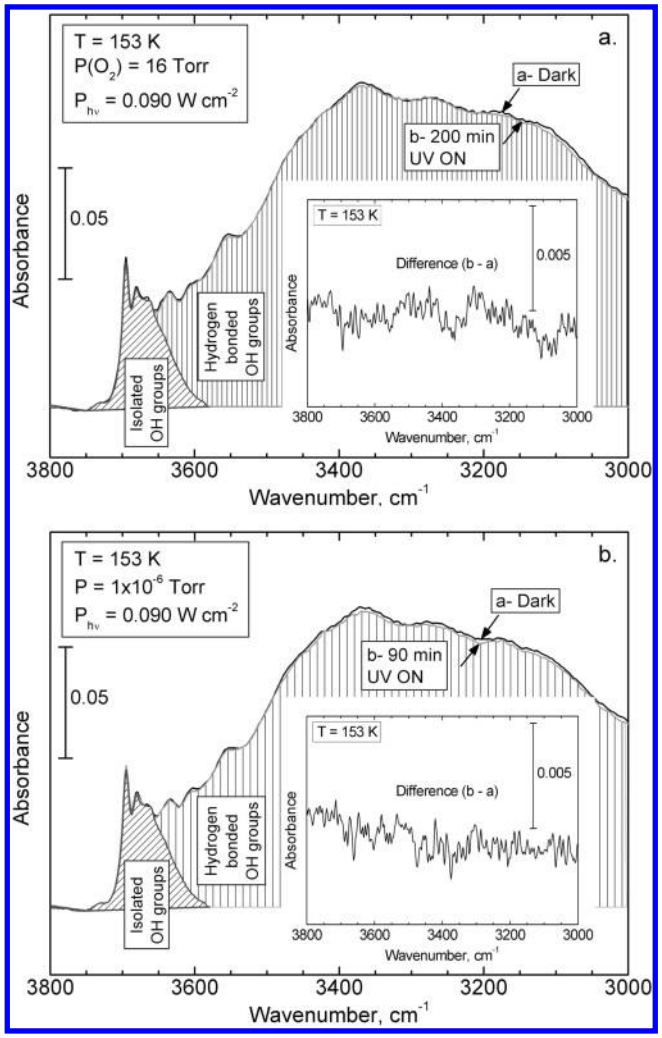

Figure 9. Absence of UV effect on the transmission IR spectra of TiO_2 after H_2O adsorption and cooling to 153 K: (a) under 16 Torr of O_2; (b) under vacuum (1×10^{-6} Torr). The insets show difference spectra under magnification.

B. Expected Adsorbed Hexane Coverages During the Experiment. Hexane gas concentrations up to 360 ppm have been employed in 1 atm of oxygen gas. The hexane flux on the surface at 360 ppm is 5.9×10^{19} cm^{-2} s^{-1}, or about 10^5 monolayers s^{-1} (ML s^{-1}). Under these conditions, at 300 K, one monolayer of hexane is likely to form, based on assumptions given in ref 33. As schematically shown in Figure 10, the adsorbed hexane is continuously photooxidized and is continuously resupplied from the gas in the experiment. Gradually, the steady-state surface concentration of adsorbed hexane diminishes as the irradiation time in O_2 increases, due to the increased rate of loss of hydrocarbon by the photooxidation process. We believe that the induction period prior to wetting is the time period where the reduction of the equilibrium surface coverage of adsorbed hexane approaches a fraction of a monolayer coverage, and that atomically clean $TiO_2(110)$ is a hydrophilic surface exhibiting a near-zero contact angle. Upon reaching this critical condition of almost perfect surface cleanliness, the water suddenly wets the TiO_2 surface beyond its perimeter, as shown schematically in Figure 11. For hydrocarbons with molecular weights higher than that of hexane, the wetting delay phenomenon should be observed at lower gas-phase hydrocarbon concentrations, due to the increased hydrocarbon binding energy to the TiO_2 surface, as deduced from the argument in ref 33. Conversely, the production of a hydrophilic oxidation product

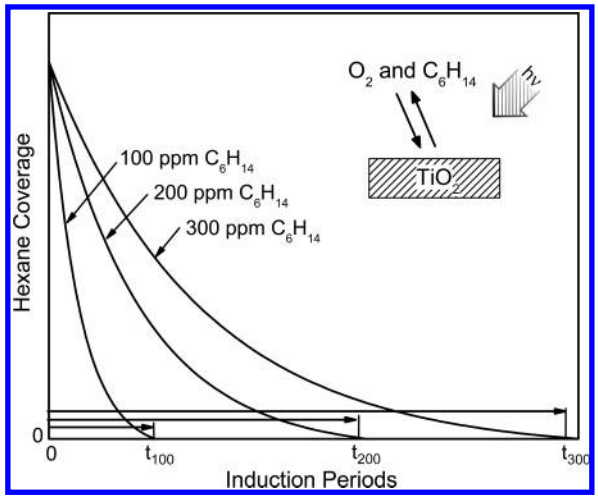

Figure 10. Schematic model of the effect of gas-phase hexane on its photooxidation kinetics on a $TiO_2(110)$ surface preceding the complete wetting with water.

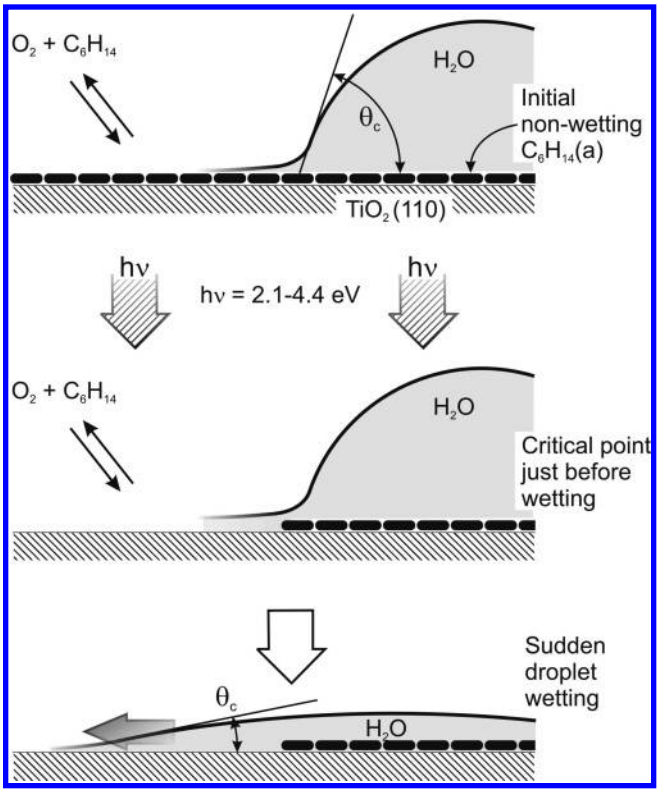

Figure 11. Schematic interpretation of the sudden hydrophilic effect due to hydrocarbon photooxidation on $TiO_2(110)$ outside the water droplet perimeter. θ_C is the macroscopically observed contact angle.

could be involved in the sudden decrease in contact angle as hexane is photooxidized on the $TiO_2(110)$ surface.

C. Screening by the Water Droplet. The schematic diagram in Figure 11 shows that the photooxidation of adsorbed hexane occurs preferentially beyond the perimeter of the water droplet. This idea is suggested by the results of Figure 7, where expansion of the droplet immediately leads to drop spreading into TiO_2 surface regions that are unshielded by liquid water during irradiation. The shielding effect by liquid water is likely related to the limited kinetic availability of dissolved O_2 at the water−TiO_2 interface, compared to the enormous O_2 flux experienced in regions of the TiO_2 surface which are not covered by liquid water. In Figure 11, we also depict a prewetting layer extending beyond the optically observed perimeter of the droplet.

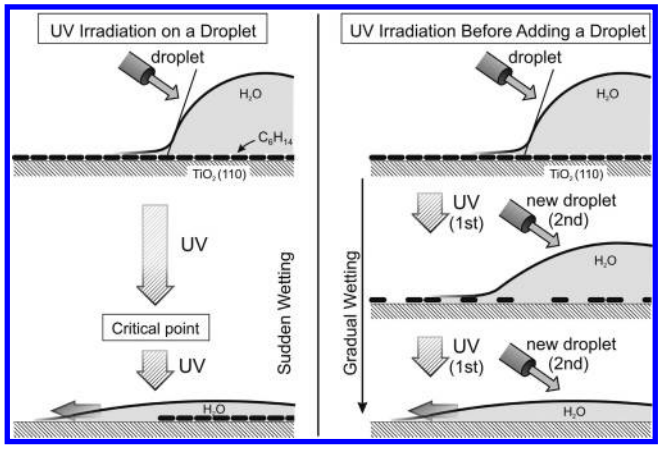

Figure 12. Comparison of TiO_2 hydrophilic conversion kinetics for two types of experiments. Left panel: sudden wetting during continuous UV irradiation of a water droplet on TiO_2. Right panel: gradual wetting observed when a new droplet of water is deposited each time after UV irradiation.

The concept of such prewetting (precursor) layers only a few monolayers thick was introduced by Bascom in 1964[34] and later confirmed for aqueous solutions.[35]

D. Lack of Photoeffects on Adsorbed H_2O and on Ti−OH Groups on TiO_2. Because of the postulate that dissociative H_2O chemistry occurs when TiO_2 vacancy defect sites are produced by UV irradiation[8,10−12,14−16] or when Ti−O bonds are broken in bridging >OH groups,[13] we employed transmission IR spectroscopy on a high-area TiO_2 surface to search for changes in the vibrational spectrum of H_2O or of Ti−OH groups following intense UV irradiation in O_2 and in a vacuum. The experiments shown in Figure 9 clearly indicate that no photochemistry occurs for H_2O or Ti−OH groups when irradiated with UV light under O_2 or in a vacuum when precautions are taken to eliminate evaporation and dehydroxylation effects by working at 153 K. These results are consistent with earlier STM measurements of the $TiO_2(1\times1)$ surface, where high-intensity UV irradiation was shown to produce no surface defects. The cross section for UV-induced defect formation is not above the very low experimental limit of $10^{-23.5}$ cm^2.[36]

E. Comparison to Experiments in Ambient Atmospheres Involving Irradiation followed by Droplet Addition. The major observation in this work is that water droplets on hydrocarbon-contaminated TiO_2 surfaces, when irradiated in an O_2 atmosphere, exhibit a wetting delay before sudden wetting occurs. In contrast, water droplets added to the TiO_2 surface after various periods of irradiation in O_2 show a gradual reduction in the contact angle. Figure 12 shows a schematic comparison of the two experiments and our explanation of the difference. In the case of our experiments, photooxidation of the surface regions which are not shielded by the water droplet leads to slow removal of the hydrocarbon layer until the surface is clean. At this critical point, the water boundary suddenly moves away from the underlying hydrocarbon layer on which it rests to wet the cleaned surface. In the case of the experiments where the unwetted surface is first exposed to UV radiation in the presence of O_2, decreasing coverages of hydrocarbon are obtained as the irradiation time increases, and added water droplets sample the hydrocarbon layer at various levels of hydrocarbon coverage,[37] giving a range of observed contact angles.

F. UV-Induced Defect Site Production on $TiO_2(110)$? The suggestion by others[8−12,14,15,38] that defect sites are produced by UV irradiation of TiO_2 is not verified by direct measurements with STM. Studies in this laboratory have demonstrated that the cross section for defect production lies below $10^{-23.5}$ cm^2 for UV photons with energies above 3.0 eV,[36] and such an upper limit of cross section is far too small to allow the UV defect model to explain the TiO_2 hydrophilicity phenomenon which is known to occur at low UV fluences. The proposed hydroxyl group production from H_2O on UV-induced defect sites[4,8−13] is, therefore, unlikely, and the IR experiments in Figure 9 confirm that no changes in the frequency or intensity of −OH groups in either Ti−OH species or in adsorbed H_2O species take place upon UV irradiation.

V. Summary of Results

These measurements of the hydrophilicity effect due to UV irradiation of TiO_2, carried out under highly controlled surface and gas-phase conditions, provide the following insights into the basic phenomenon:

1. The sudden onset of photoinduced wetting under photooxidation conditions is caused by the production of a critical surface condition at the perimeter of a water droplet which covers a hydrocarbon-coated TiO_2 surface.

2. The critical wetting condition occurs when the steady-state surface coverage of adsorbed hydrocarbons reaches zero at and beyond the water droplet perimeter as a result of complete TiO_2-mediated photooxidation of the adsorbed hydrocarbon.

3. Gas-phase O_2 is necessary to cause the photoinduced hydrophilicity effect. The photooxidation of hydrocarbons is attenuated under water droplets at the liquid water−TiO_2 interface by kinetic limitation of the O_2 supply from dissolved O_2 in the water.

4. The irradiation time (wetting delay) needed to reach the critical wetting condition increases with increased gas-phase hydrocarbon concentration as a result of increased hydrocarbon flux at the surface.

5. Infrared spectroscopy measurements indicate that neither adsorbed H_2O nor Ti−OH groups are influenced by UV irradiation in O_2 or in a vacuum. These and earlier STM experiments indicate that photoproduced hydrophilic behavior on TiO_2 does not involve the production of surface oxygen vacancy defect sites, enhanced surface Ti−OH coverages on defect sites, or the modified surface bonding of bridging >OH groups, as postulated by others.

6. The results of this experiment suggest that water contact angle experiments carried out under ambient conditions in uncontrolled atmospheres containing unknown levels of hydrocarbons will be subject to uncharacterized and possibly irregular contamination effects which limit their interpretation.

Acknowledgment. We acknowledge with thanks the support of this work by PPG Industries and by the DOD Multidisciplinary University Research Initiative (MURI) program administered by the Army Research Office under Grant DAAD 19-01-0-0619. We also personally thank Dr. Charles Greenberg and Dr. Scott Walck of PPG for their personal interest in the support of this project.

References and Notes

(1) Wang, C. Y.; Groenzin, H.; Shultz, M. J. *Langmuir* **2003**, *19*, 7330−7334.

(2) Fujishima, A.; Rao, T. N.; Tryk, D. A. *J. Photochem. Photobiol. C* **2000**, *1*, 1−21.

(3) White, J. M.; Szanyi, J.; Henderson, M. A. *J. Phys. Chem. B* **2003**, *107*, 9029−9033.

(4) Gao, Y. F.; Masuda, Y.; Koumoto, K. *Langmuir* **2004**, *20*, 3188−3194.

(5) Fujishima, A.; Hashimoto, K.; Watanabe, H. *TiO_2 Photocatalysis: Fundamentals and Applications*; BKC: Tokyo, 1999.
(6) Yin, H. Y.; Jin, Z. S.; Zhang, S. L.; Wang, S. B.; Zhang, Z. J. *Sci. China, Ser. B: Chem.* **2002**, *45*, 625−632.
(7) Watanabe, T.; Nakajima, A.; Wang, R.; Minabe, M.; Koizumi, S.; Fujishima, A.; Hashimoto, K. *Thin Solid Films* **1999**, *351*, 260−263.
(8) Wang, R.; Hashimoto, K.; Fujishima, A.; Chikuni, M.; Kojima, E.; Kitamura, A.; Shimohigoshi, M.; Watanabe, T. *Nature* **1997**, *388*, 431−432.
(9) Sun, R. D.; Nakajima, A.; Fujishima, A.; Watanabe, T.; Hashimoto, K. *J. Phys. Chem. B* **2001**, *105*, 1984−1990.
(10) Miyauchi, M.; Nakajima, A.; Fujishima, A.; Hashimoto, K.; Watanabe, T. *Chem. Mater.* **2000**, *12*, 3−5.
(11) Nakajima, A.; Koizumi, S.; Watanabe, T.; Hashimoto, K. *J. Photochem. Photobiol. A* **2001**, *146*, 129−132.
(12) Wang, R.; Sakai, N.; Fujishima, A.; Watanabe, T.; Hashimoto, K. *J. Phys. Chem. B* **1999**, *103*, 2188−2194.
(13) Sakai, N.; Fujishima, A.; Watanabe, T.; Hashimoto, K. *J. Phys. Chem. B* **2003**, *107*, 1028−1035.
(14) Miyauchi, M.; Kieda, N.; Hishita, S.; Mitsuhashi, T.; Nakajima, A.; Watanabe, T.; Hashimoto, K. *Surf. Sci.* **2002**, *511*, 401−407.
(15) Wang, R.; Hashimoto, K.; Fujishima, A.; Chikuni, M.; Kojima, E.; Kitamura, A.; Shimohigoshi, M.; Watanabe, T. *Adv. Mater.* **1998**, *10*, 135−138.
(16) Sakai, N.; Fujishima, A.; Watanabe, T.; Hashimoto, K. *J. Phys. Chem. B* **2001**, *105*, 3023−3026.
(17) Nakamura, M.; Makino, K.; Sirghi, L.; Aoki, T.; Hatanaka, Y. *Surf. Coat. Technol.* **2003**, *169*, 699−702.
(18) Thompson, T. L.; Diwald, O.; Yates, J. T., Jr. *J. Phys. Chem. B* **2003**, *107*, 11700−11704.
(19) Yates, J. T., Jr. *Experimental Innovations in Surface Science*; Springer-Verlag: New York, 1998.
(20) Wong, J. C. S.; Linsebigler, A.; Lu, G. Q.; Fan, J. F.; Yates, J. T., Jr. *J. Phys. Chem.* **1995**, *99*, 335−344.
(21) Pan, J. M.; Maschhoff, B. L.; Diebold, U.; Madey, T. E. *J. Vac. Sci. Technol., A* **1992**, *10*, 2470−2476.
(22) Fuentes, G. G.; Elizalde, E.; Yubero, F.; Sanz, J. M. *Surf. Interface Anal.* **2002**, *33*, 230−237.
(23) Childs, K. D.; Carlson, B. A.; LaVanier, L. A.; Moulder, J. F.; Paul, D. F.; Stickle, W. F.; Watson, D. G. *Handbook of Auger Electron Spectroscopy*; Physical Electronics, Inc.: 1995.
(24) Uetsuka, H.; Sasahara, A.; Onishi, H. *Langmuir* **2004**, *20*, 4782−4783.
(25) Chapman, S. *Rep. Prog. Phys.* **1943**, *9*, 92−100.
(26) Basu, P.; Ballinger, T. H.; Yates, J. T., Jr. *Rev. Sci. Instrum.* **1988**, *59*, 1321−1327.
(27) Yates, D. J. C. *J. Phys. Chem.* **1961**, *65*, 746−753.
(28) Hadjiivanov, K. I.; Klissurski, D. G. *Chem. Soc. Rev.* **1996**, *25*, 61−70.
(29) Primet, M.; Pichat, P.; Matthieu, M.-V. *J. Phys. Chem.* **1971**, *75*, 1216−1220.
(30) Jackson, P.; Parfitt, G. D. *Trans. Faraday Soc.* **1971**, *67*, 2469−2483.
(31) Tanaka, K.; White, J. M. *J. Phys. Chem.* **1982**, *86*, 4708−4714.
(32) Li, M.; Hebenstreit, W.; Gross, L.; Diebold, U.; Henderson, M. A.; Jennison, D. R.; Schultz, P. A.; Sears, M. P. *Surf. Sci.* **1999**, *437*, 173−190.
(33) Approximate estimates of the steady-state coverage of reversibly bound hexane at 300 K on TiO_2 may be made using the following argument. The incoming flux of hexane at 360 ppm will be 5.9×10^{19} cm^{-2} s^{-1}, or about 10^5 ML s^{-1}. In the absence of photooxidation, this is balanced by the desorption rate which may be approximated from the activation energy for desorption of hexane (estimated to be 43.5 kJ mol^{-1} from: Slayton, R. M.; Aubuchon, C. M.; Camis, T. L.; Noble, A. R.; Tro, N. J. *J. Phys. Chem.* **1995**, *99*, 2151−2154). Assuming a sticking coefficient of unity, the steady-state coverage of hexane is $\sim 10^{15}$ cm^{-2}, or $\sim$1 ML. Because the enthalpy of hexane vaporization from the second layer (assumed to be ΔH_{vap}(*n*-hexane)) is smaller than the activation energy for desorption, the formation of a second layer or a multilayer of hexane is unlikely under the conditions of this experiment. Thus, it is likely that the hydrophilic phenomenon occurs during the final stage of photooxidation of a monolayer or less of reversibly adsorbed hexane.
(34) Bascom, W. D.; Cottington, R. L.; Singleterry, C. R. *Adv. Chem. Ser.* **1964**, *43*, 355−379.
(35) Ghiradella, H.; Radigan, W.; Frisch, H. L. *J. Colloid Interface Sci.* **1975**, *51*, 522−526.
(36) Mezhenny, S.; Maksymovych, P.; Thompson, T. L.; Diwald, O.; Stahl, D.; Walck, S. D.; Yates Jr., J. T. *Chem. Phys. Lett.* **2003**, *369*, 152−158.
(37) Seki, K.; Tachiya, M. *J. Phys. Chem. B* **2004**, *108*, 4806−4810.
(38) Shultz, A. N.; Jang, W.; Hetherington, W. M.; Baer, D. R.; Wang, L. Q.; Engelhard, M. H. *Surf. Sci.* **1995**, *339*, 114−124.